Direct Visualization of the Gouy Phase by Focusing Phonon Polaritons

T. Feurer, Nikolay S. Stoyanov, David W. Ward, and Keith A. Nelson*

Department of Chemistry, Massachusetts Institute of Technology, Cambridge, Massachusetts 02139

(Received 9 February 2002; published 7 June 2002)

We report the generation of aberration-free cylindrical phonon-polariton wave packets in uniaxial $LiTaO_3$ crystals by nonresonant impulsive stimulated Raman scattering. The unique properties of phonon polaritons with a typical carrier frequency in the THz regime allow direct measurement of the spatiotemporal amplitude and phase distributions. We demonstrate that under these conditions the phase anomaly (Gouy phase) may be visualized directly through spatiotemporal imaging as the cylindrical wave propagates through its focus.

DOI: 10.1103/PhysRevLett.88.257402 PACS numbers: 78.47.+p, 42.25.–p

Over 100 years ago Gouy [1] discovered that a converging spherical wave obstructed by a circular aperture experiences an anomalous phase shift as it passes through the focal region. This phase shift is now called the Gouy phase shift or phase anomaly and is best known in the case of an obstructed paraxial Gaussian beam [2]. A number of years ago, it was pointed out that the Gouy phase is a special case of the topological Berry phase that parameters associated with an evolving wave, such as the phase curvature, experience as the wave propagates [3]. A more intuitive interpretation of the Gouy phase has been given in terms of a geometrical quantum effect [4] or the uncertainty principle [5]. Here the Gouy phase arises as the spatial volume available to the photon or to a wave is confined, and the wave vector distribution, via the uncertainty principle, changes accordingly. The focusing of a wave in the paraxial limit, for example, leads to a spatial confinement perpendicular to the propagation direction, and, consequently, the wave vector spread in these directions increases. This leads to a relocation of the wave vector distribution away from the forward component to the transverse components and back as the wave propagates through the focal region.

The Gouy phase plays an important role whenever focusing of a wave to the diffraction limit is considered, as in resonators, optical tweezers, or phase-sensitive nonlinear interactions of light with matter in the focus of a high intensity beam. With the advent of single cycle and even subcycle THz pulses, interest in the Gouy phase was revived because it is responsible for dramatic changes of the amplitude of those pulses as they pass through the focus. In a more general context, single and subcycle THz wave forms have triggered a growing interest in the spatiotemporal evolution of such pulses [6–13].

To date, the Gouy phase has been only indirectly observed. The first realization was performed by Gouy himself using white light interferometry [1]. Later experiments used microwaves to infer the existence of the Gouy phase [14,15]. More recent experiments with single cycle THz pulses have confirmed the predicted amplitude changes caused by the Gouy phase for cylindrical [16] and spherical [17] single cycle pulses and constitute the first noninterferometric measurements of the Gouy phase at THz frequencies.

In this Letter we report the direct observation of the Gouy phase shift through real-space imaging of a phonon-polariton wave packet passing through a focus. The curved wave front is generated through semicircular spatial excitation and is therefore aberration-free, and the phase front is parallel to the pulse front. "Snapshots" of the spatiotemporal evolution recorded by a femtosecond imaging pulse at different times following excitation allow direct visualization of the phase fronts as the wave packet moves through the focal region, thereby revealing the phase anomaly through direct observation.

The experiments were performed using a homebuilt femtosecond Ti:sapphire laser system with a repetition rate of 1 kHz, a pulse width of 50 fs, and a pulse energy of 0.7 mJ. The laser output was split into a pump and a variably delayed imaging beam. The pump beam was expanded, sent through an axicon-lens combination that yielded a ringlike focal intensity distribution, and imaged onto an x-cut 5-mm-thick $LiTaO_3$ single crystal. The diameter of the excitation ring at the sample was (2.3 ± 0.1) mm with a thickness of (0.20 ± 0.05) mm. The pulse energy at the sample was adjusted to 60 μJ, leading to an excitation intensity of (83 ± 25) GW/cm^2. For semicircular excitation, half of the ring was blocked.

A phonon-polariton mode represents an eigenmode of an ionic crystal which has both an electromagnetic and a polar lattice vibrational contribution, and which has a frequency in the THz region. In $LiTaO_3$, which is a uniaxial crystal, phonon polaritons may be driven coherently by femtosecond laser pulses through impulsive stimulated Raman scattering, with the optical and the phonon-polariton polarizations aligned parallel to the crystal axis [18]. The semicircular excitation pattern persists with good collimation throughout the depth of the sample, so the geometry is essentially two dimensional; i.e., the phonon-polariton propagation component of interest is parallel to the crystal surface and perpendicular to both the excitation and the imaging beam. The coherent phonon-polariton response modulates the index of refraction through the electro-optic

effect, and a variably delayed probe beam is used to image this modulation through phase sensitive Talbot imaging [19,20]. An important feature of the detection scheme is that the images recorded at different delay times reveal the spatiotemporal evolution of the phonon-polariton amplitude.

Figure 1 shows a sequence of snapshots taken at different delay times between the pump and the imaging pulse. The excitation ring is larger than the size of the images and not visible. Because of momentum conservation there is also an outward traveling counterpart of the phonon-polariton response which is not seen here for the same reason. Note that the phonon-polariton phase front is fully aberration-free. The phase and the pulse front curvature are solely determined by the spatial profile of the excitation laser light at the sample, and are almost perfectly circular. The initial phonon-polariton amplitude, however, is maximal when the generated wave front is parallel to and minimal when it is perpendicular to the excitation polarization direction. The central wavelength of the phonon-polariton response is about $\lambda_0 = 2\pi/k_0 \approx 165\ \mu$m, and the beam waist at the focus is approximately 55 μm. About 25 ps after excitation, the phonon-polariton wave packet passes through the focus. Obviously, the numerical aperture of the focusing wave packet is much greater than 1, and we expect that a scalar electromagnetic field description will fail to reproduce the observed phonon-polariton propagation. Therefore, finite-difference time-domain calculations of the propagating electromagnetic part of the response were performed in order to simulate its spatiotemporal evolution. The polar vibrational mode was incorporated implicitly in the dielectric constant which, for the present conditions, is essentially dispersionless. In addition, the medium was assumed to be isotropic and lossless. Anisotropy would lead to spatial distortion of the semicircular wave packet as it propagates and was not observed for $LiTaO_3$, in agreement with Ref. [21]. The simulations were performed in two spatial dimensions perpendicular to the propagation direction of the excitation laser pulse. The measured waveform just after excitation was used for the simulations as an initial condition.

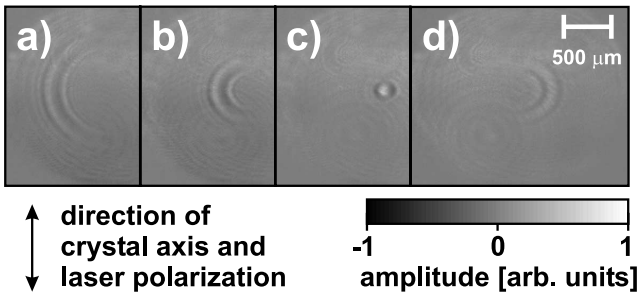

FIG. 1. Semicircular phonon-polariton wave packet propagating from left to right. The snapshots are recorded (a) 12.3 ps, (b) 18.9 ps, (c) 25.6 ps, and (d) 32.3 ps after excitation and show the phonon-polariton amplitude.

Extracting the phonon-polariton amplitude on the propagation axis from each single snapshot and stacking them next to each other yield the spatiotemporal amplitude distribution as shown in Fig. 2. With increasing delay time, the on-axis part of the wave packet propagates towards larger distances. As it passes through the focus, the peaks and valleys of the phase accelerate, propagate with superluminal phase velocity, decelerate again, and finally continue to propagate with the normal phase velocity. At the same time, the amplitude increases as the wave packet approaches the focus and decreases again as the wave packet diverges. The experimental data in Fig. 2 also confirm that damping on the length scales under consideration may be neglected.

If we trace a single phase peak and subtract the phase $k_0 z$, that is, the phase acquired due to free space propagation, any anomalous phase contribution should become obvious. The result is shown in Fig. 3. Clearly, there is an additional anomalous phase acquired as the wave packet traverses the focal region. This is the Gouy phase. Most of the additional phase is occurring within one or two Rayleigh ranges. The wave packet launched by the excitation

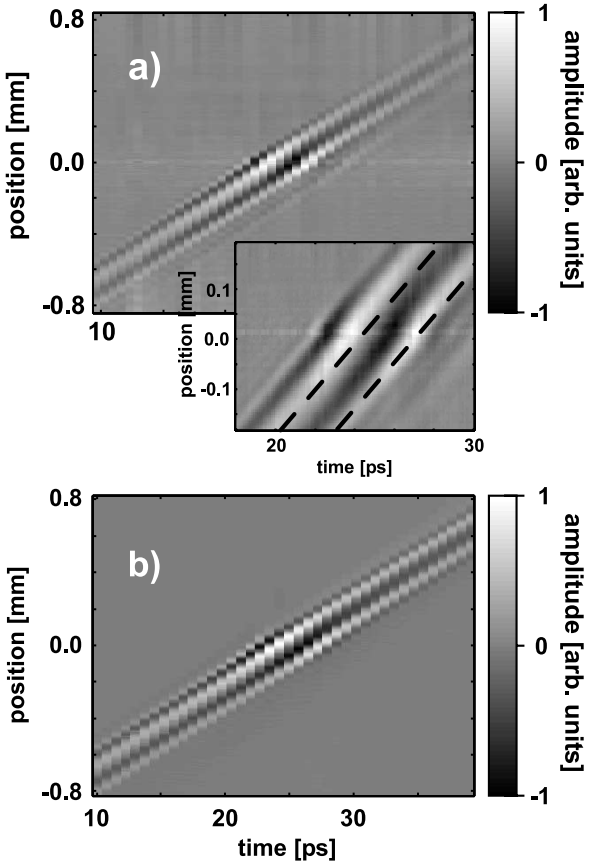

FIG. 2. Spatiotemporal distribution of the phonon-polariton amplitude. (a) Experimental data. The inset shows experimental data around the focus with a higher temporal resolution. The dashed lines indicate the phase fronts as they would evolve if there were no Gouy phase shift. (b) Finite-difference time-domain simulation.

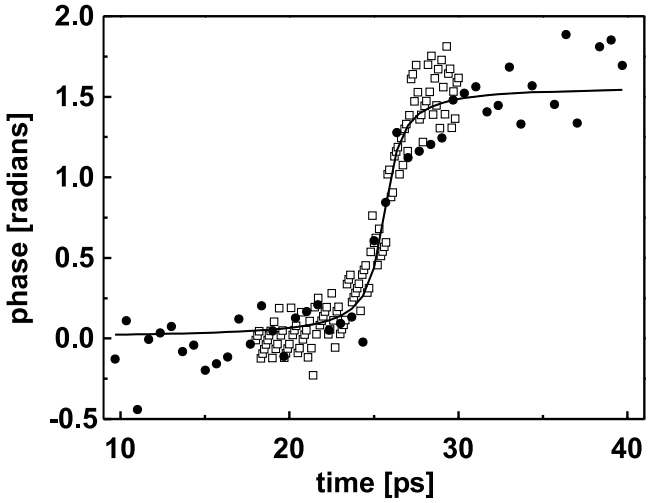

FIG. 3. Gouy phase or phase anomaly. Experimental data [solid circles and open squares correspond to the data shown in Fig. 2(a)] and finite-difference time-domain simulation (solid line).

pulse is focused in one dimension only, i.e., parallel to the optic axis of the crystal. In this case, the Gouy phase is expected to be $\pi/2$ [5], in excellent agreement with experiment.

In physical terms, the Gouy phase causes the propagation constant within the focal region to decrease and the wavelength to increase. Consequently, the phase fronts of the semicylindrical wave packet advance by a quarter of a wavelength as it passes through the focus. Recently, it has been pointed out that the physical origin of the Gouy phase shift may be explained by the uncertainty principle [5]. That is, any spatial confinement perpendicular to the wave propagation direction leads to an increasing spread in the corresponding wave vectors. Therefore, the wave vector component parallel to the axis of propagation must decrease as the perpendicular wave vector components increase. Inspection of Fig. 4 shows that as the phonon-polariton wave packet passes through the focal region, the wave vector spectrum is shifted toward smaller values. The wave vector spectrum for each delay time was obtained by calculating the Fourier transform of the spatial phonon-polariton amplitude along the axis of propagation. The same behavior is seen in the finite-difference time-domain simulations, and demonstrates the temporary increase of the wavelength or the relocation of wave vector contributions as the phonon-polariton wave packet traverses the focal region.

In conclusion, we have shown that through a specific excitation geometry it is possible to generate an aberration-free phonon-polariton wave packet with semicircular phase fronts. The pump-probe imaging scheme allows observation of the phase fronts as they propagate through the focal region and therefore direct visualization of the Gouy phase. The experimental results are in excellent agreement with numerical solution of nonscalar Maxwell's equations.

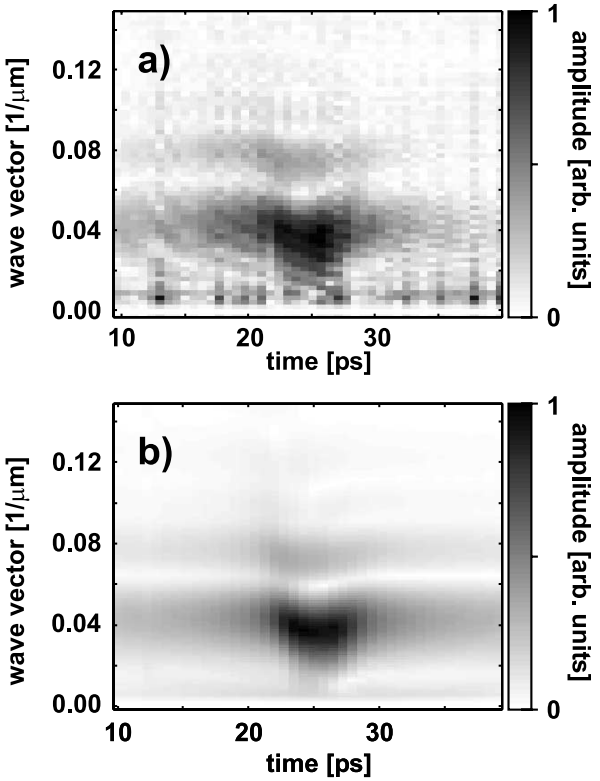

FIG. 4. Wave vector amplitude as a function of time for the wave vector component in the propagation direction. (a) Experimental data; (b) finite-difference time-domain simulation.

This work was supported in part by National Science Foundation Grant No. CHE97-13388. The authors thank Joel D. Eaves for helpful discussions. T. Feurer acknowledges financial support by the Max Kade Foundation.

*Electronic address: kanelson@mit.edu

[1] C. R. Gouy, Acad. Sci. Paris **110**, 1251 (1890).
[2] B. E. A. Saleh and M. C. Teich, *Fundamentals of Photonics* (John Wiley & Sons, Inc., New York, 1991).
[3] D. Subbarao, Opt. Lett. **20**, 2162 (1995).
[4] P. Hariharan and P. A. Robinson, J. Mod. Opt. **43**, 219 (1996).
[5] S. Feng and H. G. Winful, Opt. Lett. **26**, 485 (2001).
[6] D. You and P. Bucksbaum, J. Opt. Soc. Am. B **14**, 1651 (1997).
[7] S. Feng, H. G. Winful, and R. W. Hellwarth, Opt. Lett. **23**, 385 (1998).
[8] M. A. Porras, Phys. Rev. E **58**, 1086 (1998).
[9] S. Feng, H. G. Winful, and R. W. Hellwarth, Phys. Rev. E **59**, 4630 (1999).
[10] S. Hunsche, S. Feng, H. G. Winful, A. Leitenstorfer, M. C. Nuss, and E. P. Ippen, J. Opt. Soc. Am. A **16**, 2025 (1999).
[11] Z. L. Horvath and Zs. Bor, Phys. Rev. E **60**, 2337 (1999).
[12] S. Feng and H. G. Winful, Phys. Rev. E **61**, 862 (2000).
[13] P. Saari, Opt. Express **8**, 590 (2001).
[14] M. P. Bachynski and G. Bekefi, J. Opt. Soc. Am. **47**, 428 (1957).

[15] G. W. Farnell, Can. J. Phys. **36**, 935 (1958).
[16] R. W. McGowan, R. A. Cheville, and D. Grischkovsky, Appl. Phys. Lett. **76**, 670 (2000).
[17] A. B. Ruffin, J. V. Rudd, J. F. Whitaker, S. Feng, and H. G. Winful, Phys. Rev. Lett. **83**, 3410 (1999).
[18] T. P. Dougherty, G. P. Wiederrecht, and K. A. Nelson, J. Opt. Soc. Am. B **9**, 2179 (1992).
[19] K. Patorski, in *Progress in Optics,* edited by E. Wolf (North-Holland, Amsterdam, 1989), Vol. 27.
[20] R. M. Koehl, S. Adachi, and K. A. Nelson, J. Phys. Chem. A **103**, 10 260 (1999).
[21] M. Schall, H. Helm, and S. R. Keiding, Int. J. Infrared Millim. Waves **20**, 595 (1999).